

# Highly-Crystallized $\alpha$ -FeOOH for Stable and Efficient Oxygen Evolution Reaction

Wenjun Luo<sup>a,b,\*</sup>, Chaoran Jiang<sup>b</sup>, Yaomin Li<sup>c</sup>, Stephen A. Shevlin<sup>c</sup>, Xiaoyu Han<sup>c</sup>, Kaipei Qiu<sup>c</sup>, Yingchun Cheng<sup>a</sup>, Zhengxiao Guo<sup>c</sup>, Wei Huang<sup>a,\*</sup>, Junwang Tang<sup>b,\*</sup>

<sup>a</sup>Key Laboratory of Flexible Electronics (KLOFE) & Institute of Advanced Materials (IAM), Jiangsu National Synergetic Innovation Center for Advanced Materials (SICAM), Nanjing Tech University (NanjingTech), 30 South Puzhu Road, Nanjing 211816, P. R. China.

<sup>b</sup>Department of Chemical Engineering, University College London, London WC1E 6BT, UK

<sup>c</sup>Department of Chemistry, University College London, London WC1H 0AJ, UK

\*Email: iamwjluo@njtech.edu.cn; iamwhuang@njtech.edu.cn; junwang.tang@ucl.ac.uk

**Abstract:** It is a key challenge to explore an efficient, stable and low-cost catalyst for oxygen evolution reaction (OER). Herein, we show a facile strategy to significantly enhance electrocatalytic activity and stability of crystalline  $\alpha$ -FeOOH by rapid heat treatment. We identify that crystalline  $\alpha$ -FeOOH not only shows electrocatalytic activity is as high as the benchmark FeOOH catalyst (amorphous  $\gamma$ -FeOOH), but also the highest stability among all FeOOH electrocatalysts for OER in alkaline solutions. Our findings not only deepen the fundamental understanding of the OER process on these materials but also guide further development of new low-cost electrocatalysts for energy storage via water splitting.

## 1. Introduction

Water electrolysis is a promising approach to store intermittent renewable energy, e.g. from solar, wind and tidal sources, into clean hydrogen. <sup>[1-4]</sup> The oxygen evolution reaction (OER), a four-electron process, is the rate-limiting step in the process due to its slow kinetics and a high overpotential. It is of great significance to discover more efficient, stable and earth-abundant alternatives to these commercial electrocatalysts. Recently, the first-row transition metal oxy-hydroxides, including Fe, Co, Ni and Mn elements, have received extensive attention due to their high efficiency and low cost. <sup>[5-24]</sup> In previous studies, the OER activity of single metal oxy-hydroxides is usually considered to follow the order Ni > Co > Fe > Mn, inversely proportional to ionic radius. <sup>[7]</sup> However, most recent reports

suggested that the intrinsic OER activity follows the order of Fe > Co > Ni > Mn, by exclusion of the effect of low concentration Fe impurities in NiOOH or CoOOH. [13-16]

Since Fe is the most efficient, low cost and nontoxic element among the transition metals, it is very desirable to develop a FeOOH electrocatalyst. Unfortunately, previously reported pure FeOOH electrocatalysts are highly unstable in alkaline electrolyte at a high anodic potential, due to fast oxidization into soluble  $\text{FeO}_4^{2-}$ . [14, 17, 18] Moreover, the phase and crystallinity of electrocatalysts play key roles in their electrocatalytic performance. Previous studies suggested that  $\gamma$ -FeOOH shows higher electrocatalytic activity than  $\alpha$ -FeOOH. [19, 20] Moreover, it was concluded that an amorphous sample usually outperforms a crystalline sample [21]. This has stimulated the majority of studies on amorphous FeOOH, prepared either by electro-deposition (ED) or photoelectron-deposition methods. [18, 22-24] In this study, a facile chemical bath deposition (CBD) method was used to prepare a well-crystallized  $\alpha$ -FeOOH film. The crystallized  $\alpha$ -FeOOH after rapid heat treatment demonstrates electrocatalytic activity as high as the amorphous  $\gamma$ -FeOOH, but is much more stable. To the best of our knowledge, this crystallized  $\alpha$ -FeOOH is the most stable pure FeOOH electrocatalysts in an alkali solution, without compromising the catalytic performance.

## 2. Experimental section

### 2.1 Preparation and Heat Treatment of FeOOH Films

Crystallized  $\alpha$ -FeOOH films were prepared by a chemical bath deposition method. Aqueous solution of 0.02 M  $\text{FeSO}_4$  was used as Fe source and nothing else was added into the solution.  $\alpha$ -FeOOH films were obtained on FTO substrates (TEC 15, Pilkington NSG) after depositing at 70°C for 72h. Amorphous  $\gamma$ -FeOOH film was prepared by a conventional electrodeposition method as a reference [9, 11]. A three-electrode cell was applied to deposit the film samples. A FTO substrate, Pt mesh and SCE were used as a working electrode, a counter electrode and a reference electrode, respectively. Deposition electrolyte was aqueous solution of 0.1 M  $\text{FeSO}_4$  and 0.05 M  $\text{NaNO}_3$ .  $\gamma$ -FeOOH films were electrodeposited on FTO substrates at -0.8 V VS. SCE for 400 seconds at room temperature.

In order to shorten calcination time, a quenching method was used to heat the samples following our previous method. [25] The samples were directly put into a muffle furnace with different temperatures, directly taken out and quenched to room temperature quickly.

### 2.2 Characterization of Samples

The crystal structures of the films were measured by grazing incidence X-ray diffraction (GIXRD, Bruker D8 Advance with  $\text{CuK}\alpha$  radiation ( $\lambda=1.54 \text{ \AA}$ ) equipped with a PSD

LynxEye silicon-strip detector). The morphologies of samples were examined with a scanning electron microscope (SEM, JEOL JSM-7401F). The binding energies of Fe2p and O1s in different depths of the samples were investigated by X-ray photoelectron spectroscopy (XPS, Thermo Scientific K-alpha). The binding energy was calibrated by C1s (284.8 eV) and relative concentrations of different oxygen was calculated with the CasaXPS software. Raman spectra were measured by a laser Raman spectrophotometer (Renishaw InVia) for excitation wavelengths of 514 nm. After stability measurement, the pH of KOH aqueous solution was adjusted to 0 with HCl solution and Fe<sup>3+</sup> was analysed by ICP (Thermo Scientific, iCAP6000).

### **2.3 Electrochemical Properties Measurement**

The electrochemical properties of the samples were tested in a three-electrode cell at room temperature using an electrochemical analyzer (Ivium technology). The electrolyte was 1 M KOH aqueous solution (pH~14). A FeOOH film, Pt mesh and SCE were used as a working electrode, a counter electrode and a reference electrode, respectively. Cyclic voltammetry was performed with a scan rate of 10 mV s<sup>-1</sup>. A RHE potential was calculated following the formula:  $V_{\text{RHE}} = V_{\text{SCE}} + 0.059\text{pH} + 0.241$ . No iR correction facility was employed. The electrochemical impedance spectra (EIS) of the samples were measured using with a 10 mV amplitude perturbation. Faradaic efficiency of oxygen was measured as follows. Before a Faradaic efficiency measurement, the cell was sealed and purged by Ar for half an hour until no O<sub>2</sub> or N<sub>2</sub> was detected. Evolved O<sub>2</sub> was detected by an off-line gas chromatograph with a TCD detector (Varian 430).

### **2.4 Simulation method**

The interactions between  $\alpha$ -FeOOH (goethite) surfaces and water were investigated using periodic Density Functional Theory (DFT) implemented in the VASP code<sup>[26]</sup>. A plane wave cutoff of 520 eV was selected, with the Projector Augmented Wave method used to treat core electrons<sup>[27]</sup>. A semicore projector was used for Fe, including *p* and *s* states. The GGA+U approach was used to provide an accurate treatment of localised electron states, with  $U_{\text{eff}}$  set to 5.0 eV<sup>[28]</sup>. The details can be found in Supporting Information.

## **3.Results and Discussion**

### **3.1 Crystal structures and crystalline of $\alpha$ -FeOOH by CBD and $\gamma$ -FeOOH by ED**

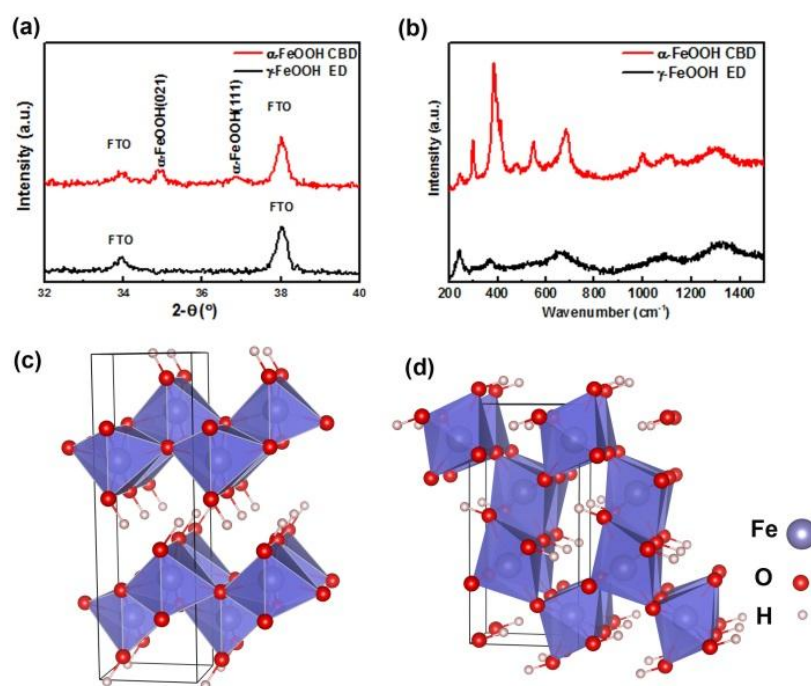


Figure 1 XRD (a) and Raman spectra (b) of as-deposited FeOOH thin films by ED and CBD methods, respectively; Crystal structures of  $\gamma$ -FeOOH (c) and  $\alpha$ -FeOOH (d).

In principle, it is more appropriate to investigate intrinsic activity of an electrocatalyst on a thin film than a powder sample to minimize the influences of extrinsic factors, such as geometric surface area, mass and electron transport.<sup>[5]</sup> Since the most efficient FeOOH electrocatalysts were prepared by the ED method in previous studies, herein, we focus on comparing electrocatalytic activity and stability between a well-crystallized  $\alpha$ -FeOOH by the CBD method and  $\gamma$ -FeOOH by the ED method. Figure 1 shows XRD patterns and Raman spectra of the as-deposited  $\gamma$ -FeOOH and the  $\alpha$ -FeOOH films, respectively. No evident diffraction peaks are observed in the ED sample (Figure 1 (a)), indicating that the prepared FeOOH film is amorphous, in agreement with previous reports using similar ED methods<sup>[11, 15, 20, 22-24]</sup>. In contrast, two evident peaks exist for the CBD sample, which can be assigned to (021) and (111) of an  $\alpha$ -FeOOH (JCPDS No. 29-0713). The intensity ratio of peak (021) to (111) is 0.3 in a random  $\alpha$ -FeOOH polycrystal, and it is 1.7 in this sample, indicating preferred orientation along (021). Raman spectra were further used to characterize the samples due to its sensitivity in short range (see Figure 1 b). Clearly broad Raman peaks of  $\gamma$ -FeOOH can be observed in the ED sample<sup>[29]</sup>; however, sharp Raman peaks of  $\alpha$ -FeOOH are observed on the CBD sample<sup>[29]</sup>, in agreement with the XRD results. In other words, an amorphous  $\gamma$ -FeOOH and a crystalline  $\alpha$ -FeOOH have been successfully prepared for comparative study. Crystal structures of  $\gamma$ - and  $\alpha$ -FeOOH are shown in Figures 1(c) and (d),

respectively. The  $\gamma$  phase is a layered structure of double chains of  $\text{Fe}(\text{O},\text{OH})_6$  octahedra with shared edges, and the layers are held together by hydrogen bonds. The  $\alpha$  phase can be described as parallel double chains of edge-sharing  $\text{Fe}(\text{O},\text{OH})_6$  octahedra and linked to neighboring double chains by corner sharing. The crystal structure of  $\alpha$ -FeOOH indicates it is thermodynamically more stable than  $\gamma$ -FeOOH. [30]

### 3.2 Effects of rapid heat treatment on OER activities of $\alpha$ -FeOOH and $\gamma$ -FeOOH

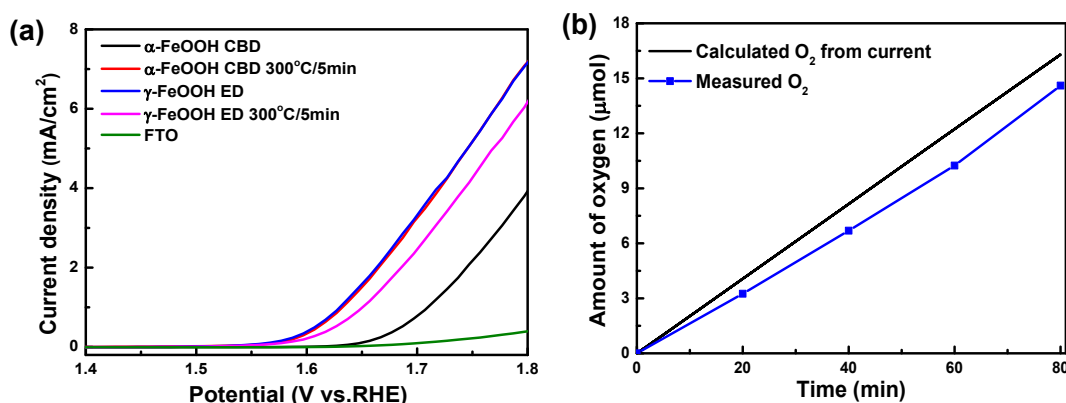


Figure 2 (a) Electrocatalytic activities of amorphous  $\gamma$ -FeOOH and crystalline  $\alpha$ -FeOOH before and after calcination at 300°C/5min in air; Electrolyte: 1 M KOH aqueous solution, scan rate: 10 mV/s, without iR-correction. (b) Faradic efficiency of O<sub>2</sub> on  $\alpha$ -FeOOH after calcination at 300°C for 5min. Electrolyte: 1M KOH aqueous solution, potential: 1.65 V<sub>RHE</sub>.

In this study, we found that rapid heat treatment had significant effect on electrocatalytic activities of the as-deposited samples and the results are shown in Figure 2 (a). The onset potential (50  $\mu\text{A}/\text{cm}^2$ ) of the as-deposited amorphous  $\gamma$ -FeOOH film is about 1.54 V<sub>RHE</sub>, close to a reported value. [11] However, the as-deposited  $\alpha$ -FeOOH sample indicates a much higher onset potential, about 1.63 V<sub>RHE</sub>, which suggests an inferior electrocatalytic performance to the amorphous  $\gamma$ -FeOOH film, in agreement with the literature. [20] After calcination at 300°C for 5 min in air, an onset potential of  $\alpha$ -FeOOH cathodically shifts about 80 mV, to a similar level to the  $\gamma$ -FeOOH. The current density increases about 50-fold at 1.6 V<sub>RHE</sub>, compared with the as-prepared  $\alpha$ -FeOOH. Faradic efficiency of O<sub>2</sub> is close to 90% at 1.65 V<sub>RHE</sub> (Figure 2b), which confirms that a lower onset potential after heat treatment is from oxygen evolution reaction. On the contrary, an onset potential of the  $\gamma$ -FeOOH shifts anodically and the corresponding current density at 1.6 V<sub>RHE</sub> decreases by about 40% after the same heat treatment.

In order to elucidate the mechanism of the rapid heat treatment enhanced electrocatalytic activity, different characterizations were carried out on the  $\alpha$ - and the  $\gamma$ -FeOOH before and after calcination at 300°C for 5 min. From XRD (Figure S1a), Raman (Figure S1b) and SEM (Figure S2) results, there are no new phases and evident morphology variation, which is reasonable, given the very short heat treatment time. Moreover, we measured the electrochemical surface area of the samples before and after the heat treatment (See Figure S3). The results suggest that there is little change in the surface area of the two samples, which means the electrochemical area does not contribute to the improved activity.

### 3.3 A possible mechanism for enhanced OER activity on $\alpha$ -FeOOH by rapid heat treatment

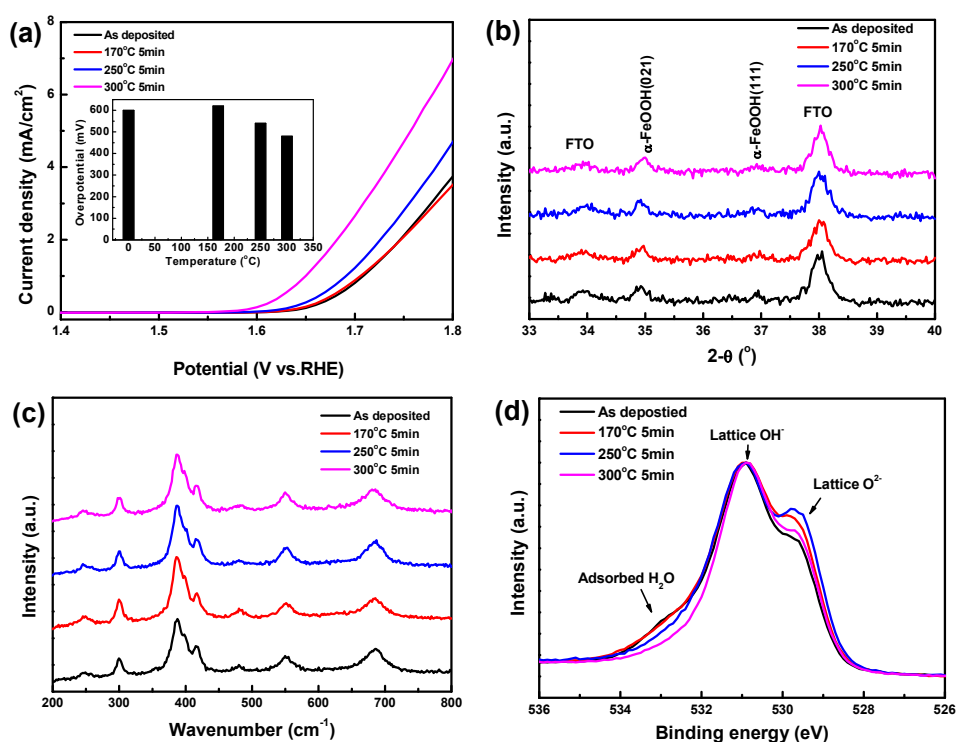


Figure 3 (a) Electrocatalytic activities of the  $\alpha$ -FeOOH samples calcined at different temperatures for 5 min; Electrolyte: 1 M KOH aqueous solution, scan rate: 10 mV/s, without iR-correction. Inset figure, overpotential (10 mA/cm<sup>2</sup>) vs. calcination temperatures, with iR-correction. (b) XRD patterns and (c) Raman spectra of the  $\alpha$ -FeOOH samples calcined at different temperatures for 5 min. (d) XPS of O1s on the surfaces of the  $\alpha$ -FeOOH calcined at different temperatures for 5 min

In order to investigate the mechanism of improved activity after rapid heat treatment, the as-deposited  $\alpha$ -FeOOH samples were calcined at different temperatures for 5 min and the

electrocatalytic activities are shown in Figure 3 (a). The activity of the  $\alpha$ -FeOOH does not increase after calcined at 170°C for 5min. Even though the sample was calcined at 170°C for a much longer time (12h), the activity of the sample still did not increase (not shown here). However, the activities of the  $\alpha$ -FeOOH sample increase after calcined at higher temperatures (250°C and 300°C) for 5min. The results suggest that there is a critical temperature to activate the as-deposited  $\alpha$ -FeOOH. Different characterization, including XRD, Raman and XPS were used to investigate variation of the samples and the results are shown in Figure 3 (b), (c) and (d) respectively. From XRD and Raman results, phase and crystalline of the  $\alpha$ -FeOOH samples do not change after calcined at 300°C or lower temperatures. In order to investigate the thermal decomposition of  $\alpha$ -FeOOH, a TG curve of the sample was measured and the result is shown in Figure S4. The result is in agreement with previous report.<sup>[31]</sup> When the sample was calcined at temperature lower than 230°C, physically adsorbed water evaporates, leading to gradual weight loss. A sharp weight loss is observed in the range of 230°C to 300°C, which are assigned to dehydration of chemically bonded water, including in the bulk and on the surface. The FeOOH samples became  $\alpha$ -Fe<sub>2</sub>O<sub>3</sub> when they were calcined at 300°C for 30 min and 60 min (see Figure S5). Here, we focus on comparing the activity and stability of  $\alpha$ -FeOOH and  $\gamma$ -FeOOH. Therefore, a longer calcination time is out of the scope of this study.

XPS was then used to provide surface information of the  $\alpha$ -FeOOH samples before and after calcination at 300°C or lower temperatures. The binding energies of Fe2p in the two samples remain similar after the rapid heat treatment, while the binding energies of O1s change (see Figure S6). Three binding energies of O1s (529.4 eV, 530.8 eV and 532.2 eV) are observed on the surface of the as-deposited  $\alpha$ -FeOOH sample, which are assigned to O<sup>2-</sup> species, OH<sup>-</sup> group and adsorbed H<sub>2</sub>O molecules, respectively (see Figure S7).<sup>[32]</sup> Also, the XPS spectra of O1s at different depths in the  $\alpha$ -FeOOH sample were measured. Peaks of water molecules decrease markedly at a depth of 5 nm into the as-deposited  $\alpha$ -FeOOH, which suggests that most water molecules exist on the surface of the sample (see Figure S8). Figure 3d shows the XPS of O1s on the surfaces of the  $\alpha$ -FeOOH after calcined at different temperatures for 5 min. Surface adsorbed water on the as-deposited  $\alpha$ -FeOOH sample does not change after calcination at 170°C, and decreases after the rapid heat treatment at 250 and 300°C for 5 min. If the calcination temperature is not high enough, it is impossible to remove the surface chemically adsorbed water, which is in agreement with the TG result. In contrast, less adsorbed water molecules are observed on the surface of the  $\gamma$ -FeOOH,

which does not change after the rapid heat treatment (see Figures S9). Previous studies suggest that the adsorption energy of molecular water on the surface of  $\alpha$ -FeOOH was much lower than on  $\gamma$ -FeOOH and water was more readily chemisorbed on the surface of  $\alpha$ -FeOOH than  $\gamma$ -FeOOH. [33, 34] Therefore, removing surface adsorbed water is a possible reason for improved activity of  $\alpha$ -FeOOH after heat treatment.

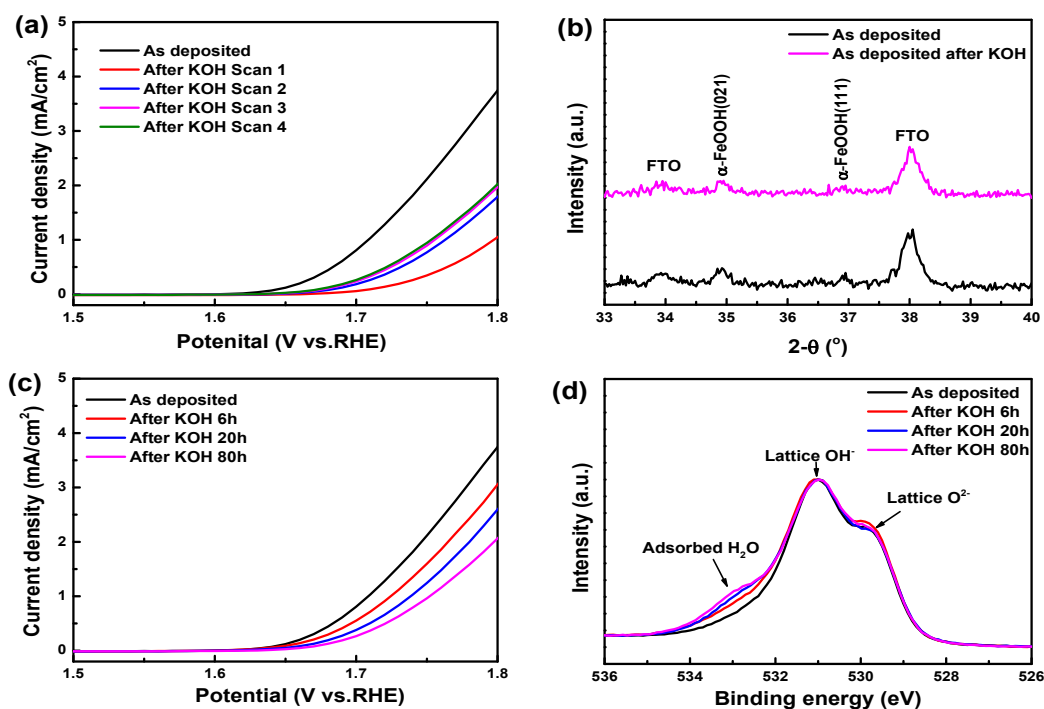


Figure 4 (a) Electrocatalytic activities of the as-deposited  $\alpha$ -FeOOH without calcination before and a sample soaked in KOH aqueous solution for 80h; (b) XRD patterns of the as-deposited  $\alpha$ -FeOOH before and after aged in KOH aqueous solution for 80h; (c) Electrocatalytic activities of the as-deposited  $\alpha$ -FeOOH and the sample soaked in KOH aqueous solution for different times; (d) XPS of O1s on the surface the as-deposited  $\alpha$ -FeOOH before and after aged in KOH aqueous solution for different times. Electrolyte: 1 M KOH aqueous solution, scan rate: 10 mV/s, without iR-correction.

In order to further investigate the effect of surface chemically bonded water on the electrocatalytic activity of the  $\alpha$ -FeOOH sample. The as-deposited  $\alpha$ -FeOOH without calcination was soaked in 1M KOH aqueous solution for different times at room temperature. Figure 4(a) indicates the electrocatalytic activity of the as-deposited  $\alpha$ -FeOOH before and after soaked in aqueous solution for 80 h. Since the sample is not calcined at high temperature, no any phase transition happens in the  $\alpha$ -FeOOH sample (see Figure 4b). The

electrocatalytic activity of the  $\alpha$ -FeOOH sample after soaked in aqueous solution decreases so much and the onset potential shifts to positive (see Figure 4a). Moreover, the electrocatalytic activity of the soaked sample was the lowest when measured for the first scan, obviously increased for the second scan, and then kept constant after the third scan. Even though, the stable performance of the  $\alpha$ -FeOOH sample after soaked in the aqueous solution is still much lower than the sample before soaked. When the  $\alpha$ -FeOOH was soaked in the aqueous solution, water was physically and chemically adsorbed on the surface of  $\alpha$ -FeOOH, respectively. The physically adsorbed water can be removed easily when the sample is measured at a high anodic potential. However, the chemically adsorbed water is very robust and cannot be removed by the anodic potential, which will cover on surface active sites of  $\alpha$ -FeOOH and decrease the activity of the sample. The stable activities (after 4 scans) of the samples soaked in the aqueous solution for different times were also measured and the results are shown in Figure 4c. Obviously, the electrocatalytic activities of the  $\alpha$ -FeOOH decrease with increasing the soaking time. Meanwhile, the concentration of surface adsorbed water increases with increasing the soaking time (see Figure 4d). Therefore, our results suggest the more chemically adsorbed water on the surface  $\alpha$ -FeOOH, the worse activity is.

Water adsorption properties of the (021) surface of the  $\alpha$ -FeOOH are simulated by Density Functional Theory (DFT) to understand the relationship between the activity of  $\alpha$ -FeOOH with surface chemically adsorbed water, see Figures 5 (a) and (b). The calculation details and the qualitative analysis are demonstrated in the Supporting Information. This (021) surface was chosen as it is the preferred orientation suggested by the XRD pattern, Figure 1a. This surface exposes Fe atoms with only five Fe-O bonds, where an Fe-O<sub>6</sub> octahedra is cleaved in half with the removal of one apex oxygen atom. There are two Fe sites, where Fe binds to three protonated oxygens (A site), and where Fe binds to two protonated oxygens (B site) (see Figure 5 (a)). Initial water adsorption is expected to be dissociative in the A site, with adsorbed OH<sup>-</sup> binding to the fivefold Fe, and the proton binding to an adjacent bridging surface oxygen. This has an exothermic reaction free energy of  $-1.038$  eV/H<sub>2</sub>O. This is a strong chemisorption, and is reflective of the chemical bond formed between the OH and Fe. The second water molecule then binds in molecular form to the B site. In contrast to the first hydroxylation, there is a significant reduction in the reaction energy for the second hydroxylation, at  $-0.620$  eV/H<sub>2</sub>O, this binding is still significant. From inspection, we note that the Fe-O distance is significantly longer than bulk, at  $2.415$  Å compared to the bulk value of  $2.057$  Å, suggesting that no chemical bond has formed.

Rather, we note the presence of significant hydrogen bonding, as indicated by a short O...H bond length of 1.643 Å, and charge density difference analysis. A hydrogen bond forms between the H<sub>2</sub>O molecule and the surface oxygens. Hydrogen-bonded adsorbed water is robust on this surface and cannot be split under an anodic potential, which prevents adsorption and oxidization of OH<sup>-</sup> on the B site in an alkali solution and limits the activity of α-FeOOH. After hydrogen-bonded adsorbed water is removed, allowing the interaction of OH<sup>-</sup> (in alkali solutions) with the B sites, increasing the active site density on the surface of α-FeOOH and leading to higher activity (see Figure 5c).

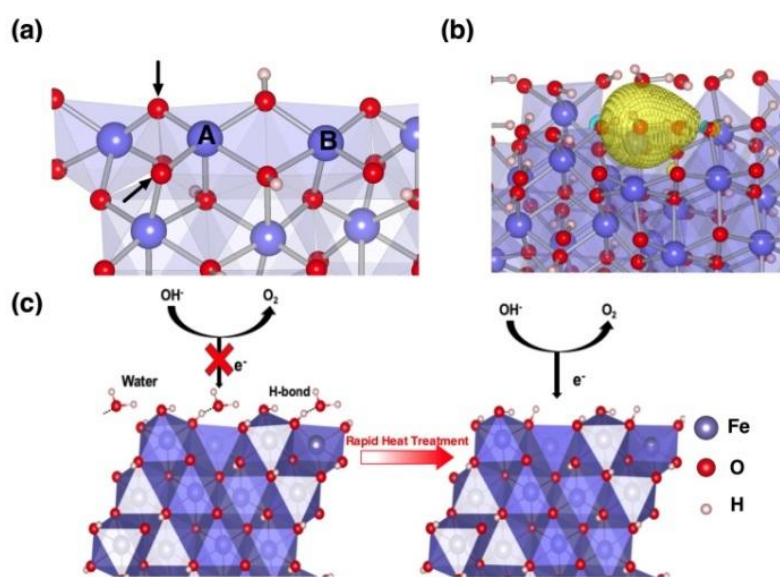


Figure 5 (a) Illustration of the (021) surface of α-FeOOH. Two different undercoordinated Fe sites, A and B, are distinguished by binding to number of protonated oxygens. Arrows indicate surface bridging oxygen. (b) Charge density difference for the second molecular hydroxylation on the (021) surface. Yellow represents charge accumulation, blue charge depletion. The isosurface contour is drawn at 0.005 e/Å<sup>3</sup>. (c) A proposed mechanism for improved electrocatalytic activity of α-FeOOH after rapid heat treatment.

### 3.4 Stability of $\alpha$ -FeOOH and $\gamma$ -FeOOH in 1M KOH aqueous solution after rapid heat treatment

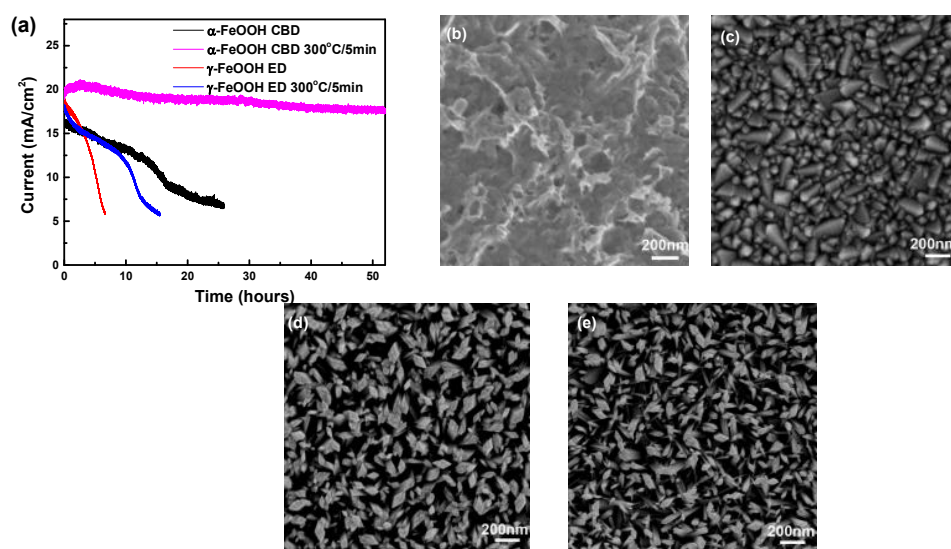


Figure 6 I-t curves of  $\alpha$ -FeOOH and  $\gamma$ -FeOOH before and after calcination at 300°C for 5 min (a). SEM images of as-deposited  $\gamma$ -FeOOH method before (b) and after (c) i-t; SEM images of as-deposited  $\alpha$ -FeOOH method before (d) and after (e) i-t; Electrolyte: 1M KOH aqueous solution, Potential: 2.1  $V_{RHE}$ .

Apart from a highly efficient  $\alpha$ -FeOOH, stability is the other key factor for practical applications for OER. Hereafter, we investigated the stability of the  $\alpha$ -FeOOH and compared it with the widely used  $\gamma$ -FeOOH. Figure 6 (a) indicates accelerated aging curves at a high potential of 2.1  $V_{RHE}$ . For the as-deposited  $\gamma$ -FeOOH, the current decreases very quickly, and all  $\gamma$ -FeOOH were dissolved into the electrolyte and no  $\gamma$ -FeOOH sample only bare FTO substrates can be observed after 8h i-t measurement (see Figures 6 b and c). The results are in good agreement with previous studies that FeOOH by ED method is easily oxidised to soluble  $FeO_4^{2-}$  at a high anodic potential in an alkaline solution, which hinders the application of FeOOH as a robust electrocatalyst. [17, 18] It is interesting to note that the stability of  $\gamma$ -FeOOH increases a little after the heat treatment, however, it is still completely dissolved after 15 h i-t measurement. Therefore, heat treatment cannot prevent the amorphous  $\gamma$ -FeOOH dissolving into the alkaline electrolyte. For the as-deposited  $\alpha$ -FeOOH, the current density decreases more slowly than the as-deposited  $\gamma$ -FeOOH. However, SEM results indicate no morphology variation on the as-deposited  $\alpha$ -FeOOH after i-t measurement (see Figure 6 d and e). Moreover, XRD and Raman further confirm the stability of the

as-deposited  $\alpha$ -FeOOH sample as no structure change is evident (see Figure S10). After i-t measurement, the adsorbed water concentration on the surface of as-deposited  $\alpha$ -FeOOH increases from 20% to 27%. Indeed, we found that the current could be mostly recovered when the as-deposited sample after i-t measurement was calcined at 300°C for 5 min. Moreover, ICP results suggest that about 3%  $\text{Fe}^{3+}$  ions to the bulk were dissolved into the solution after stability measurement. Therefore, the current decrease of the as-deposited  $\alpha$ -FeOOH comes from re-adsorption of chemically bonded water on the surface and trace dissolution of the sample. The electrocatalytic stability of the as-deposited  $\alpha$ -FeOOH sample was remarkably improved after the rapid heat treatment, and only decreased about 10% after 52 h at such a high anodic potential of 2.1  $V_{\text{RHE}}$  (See Figure 6a). In contrast, the current of  $\gamma$ -FeOOH with the same heat treatment decreases 10% only for 1.3 h measurement. The results suggest the treated crystalline  $\alpha$ -FeOOH reveals a 40 times longer lifetime than that of amorphous  $\gamma$ -FeOOH. To our best knowledge, the crystallized  $\alpha$ -FeOOH after heat treatment indicates the highest stability among all reported pure FeOOH electrocatalysts for oxygen evolution reaction in an alkali solution. [14, 16-18, 35] The higher stability of the  $\alpha$ -FeOOH than the  $\gamma$ -FeOOH is due to higher crystallinity and a more stable phase.

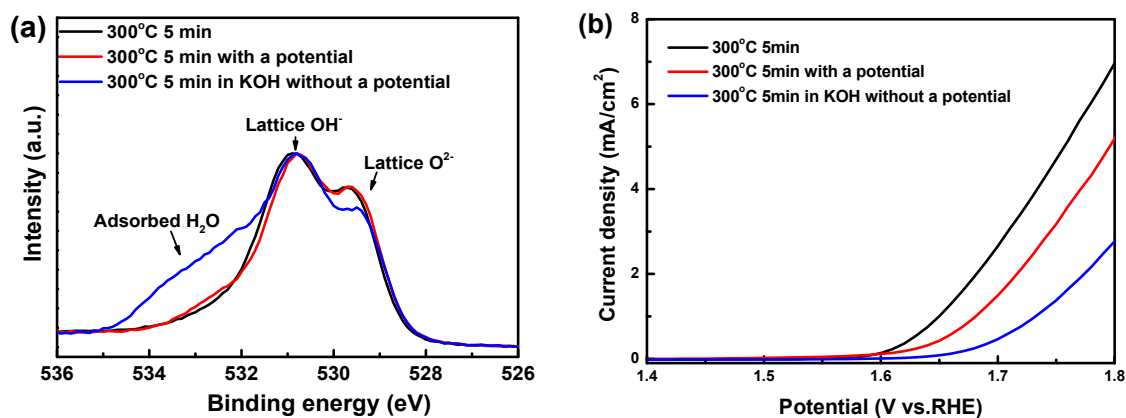


Figure 7(a) XPS of O1s on the surfaces of  $\alpha$ -FeOOH calcined at 300°C for 5 min before and after 52 h i-t measurement with a potential of 2.1  $V_{\text{RHE}}$  and aged in 1M KOH aqueous solution for 52h without a potential, respectively. (b) Electrocatalytic activities of  $\alpha$ -FeOOH calcined at 300°C 5 min before and after 52 h i-t measurement with a potential and aged in 1M KOH aqueous solution for 52 h without a potential, respectively. Electrolyte: 1 M KOH aqueous solution, scan rate: 10 mV/s, without iR-correction.

It is critical to ensure  $\alpha$ -FeOOH OER electrocatalysts to resist water re-adsorption on the heat treated surface of sample during electrochemical measurement in an aqueous solution. Here, we investigated the effect of a bias on surface water re-adsorption on the  $\alpha$ -FeOOH sample and the results are shown in Figure 7. When a heat-treated  $\alpha$ -FeOOH was soaked in a 1M KOH aqueous solution for 52 h without an anodic potential, water was re-adsorbed on the surface of the sample very easily (see Figure 7a) and the activity of the heat-treated  $\alpha$ -FeOOH decreased dramatically (see Figure 7b). However, when an anodic potential was applied on the heat-treated sample, XPS measurement indicates much less lower surface adsorbed water on the sample than that without an anodic potential. Therefore, the anodic potential can substantially prevent water re-adsorption chemical on the surface of  $\alpha$ -FeOOH in an aqueous solution. It is possible that the potential facilitates the oxidation of OH<sup>-</sup> ions to O<sub>2</sub>, thus providing a clean surface for subsequent water adsorption.

#### **4. Conclusion**

In summary, a reproducible and economic method was used to prepare crystallized  $\alpha$ -FeOOH OER electrocatalyst. The current density of crystallized  $\alpha$ -FeOOH increases by about 50-fold at 1.6 V<sub>RHE</sub> after rapid heat treatment. The crystallized  $\alpha$ -FeOOH sample after rapid heat treatment demonstrates electrocatalytic activity as high as amorphous  $\gamma$ -FeOOH but a 40 times longer. The improved electrocatalytic activity is possibly attributed to the removal of surface chemically adsorbed water. Our strategy of removing surface water by rapid heat treatment means that  $\alpha$ -FeOOH a promising OER electrocatalyst. This study also deepens the understanding of OER at interfaces between electrocatalyst and water.

#### **Acknowledgements**

The authors thank Jijia Xie and Yiou Wang for their help in Faradaic efficiency measurement. This work is financially supported by the National Basic Research Program of China (973 Program, Nos. 2015CB932200, 2014CB239303 and 2013CB632404), the Natural Science Foundation of Jiangsu Province of China (15KJB150010). Wenjun Luo, Wei Huang and Junwang Tang acknowledge a Newton Research Collaboration Programme Type 2 Award (No. NRCP/1415/264). Chaoran Jiang and Yaomin Li acknowledge financial support from China Scholarship Council (CSC File No. 201308060090 and 201406370157). Stephen Shevlin acknowledges financial support from the EU-FP7 Project NANOSIM (604656).

## Notes and references

- [1] Walter, M. G., Warren, E. L., McKone, J. R., Boettcher, S. W., Mi, Q., Santori, E. A., Lewis, N. S. *Chem. Rev.* 110, 6446-6473 (2010).
- [2] Kanan, M. W., Nocera, D. G. *Science* 321, 1072-1075 (2008).
- [3] Suntivich, J., May, K. J., Gasteiger, H. A., Goodenough, J. B., Shao-Horn, Y. *Science* 334, 1383-1385 (2011).
- [4] Luo, J., Im, J. H., Mayer, M. T., Schreier, M., Nazeeruddin, M. K., Park, N. G., Tilley, S. D., Fan, H. J., Grätzel, M. *Science* 345, 1593-1596 (2014).
- [5] Burke, M. S., Enman, L. J., Batchellor, A. S., Zou, S., and Boettcher, S. W. *Chem. Mater.* 27, 7549-7558 (2015).
- [6] Lyons, M. E. G.; Brandon, M. P. *J. Electroanal. Chem.* 641, 119-130 (2010).
- [7] Subbaraman, R., Tripkovic, D., Chang, K.-C., Strmcnik, D., Paulikas, A. P., Hirunsit, P., Chan, M., Greeley, J., Stamenkovic V. and Markovic, N. M. *Nat. Mater.* 11, 550-557 (2012).
- [8] Gong, M., Li, Y., Wang, H., Liang, Y., Wu, J. Z., Zhou, J., Wang, J., Regier, T., Wei, F. and Dai, H. *J. Am. Chem. Soc.* 135, 8452-8455 (2013).
- [9] Louie, M. W. and Bell, A. T. *J. Am. Chem. Soc.* 135, 12329-12337 (2013).
- [10] McCrory, C. C. L., Jung, S., Ferrer, I. M., Chatman, S. M., Peters, J. C. and Jaramillo, T. F. *J. Am. Chem. Soc.* 137, 4347-4357 (2015).
- [11] Swierk, J. R., Klaus, S., Trotochaud, L., Bell, A.T. and Tilley, T. D. *J. Phys. Chem. C* 119, 19022-19029 (2015).
- [12] Zhang, B., Zheng, X., Voznyy, O., Comin, R., Bajdich, M., García-Melchor, M., Han, L., Xu, J., Liu, M., Zheng, L., Arquer, F. P. G., Dinh, C. T., Fan, F., Yuan, M., Yassitepe, E., Chen, N., Regier, T., Liu, P., Li, Y., Luna, P. D., Janmohamed, A., Xin, H. L., Yang, H., Vojvodic, A., Sargent, E. H. *Science* 352, 333-337 (2016).
- [13] Trotochaud, L., Young, S. L., Ranney, J. K., Boettcher, S. W., *J. Am. Chem. Soc.* 136, 6744-6753 (2014).
- [14] Burke, M. S., Kast, M. G., Trotochaud, L., Smith, A. M., Boettcher, S. W., *J. Am. Chem. Soc.* 137, 3638-3648 (2015).
- [15] Friebel, D., Louie, M. W., Bajdich, M., Sanwald, K. E., Cai, Y., Wise, A. M., Cheng, M.-J., Sokaras, D., Weng, T.-C., Alonso-Mori, R., Davis, R.C., Bargar, J. R., Nørskov, J. K., Nilsson, A. and Bell, A. T. *J. Am. Chem. Soc.* 137, 1305-1313 (2015).
- [16] Burke, M. S., Zou, S., Enman, L. J., Kellon, J. E., Gabor, C. A., Pledger, E. and Boettcher, S. W. *J. Phys. Chem. Lett.* 6, 3737-3742 (2015).

- [17] Zou, S., Burke, M. S., Kast, M. G., Fan, J., Danilovic, N. and Boettcher, S. W. *Chem. Mater.* 27, 8011-8020 (2015).
- [18] Chemelewski, W. D., Rosenstock J. R. and Mullins, C. B. *J. Mater. Chem. A* 2, 14957-14962 (2014).
- [19] Elizarova, G. L., Zhidomirov, G.M., Parmon, V. N. *Catal. Today* 58, 71-88 (2000).
- [20] Seabold, J. A. and Choi, K.-S. *J. Am. Chem. Soc.* 134, 2186-2192 (2012).
- [21] Smith, R. D. L., Prévot, M. S., Fagan, R. D., Zhang, Z., Sedach, P. A., Siu, M. K. J., Trudel, S., Berlinguette, C. P. *Science* 340, 60-63 (2013).
- [22] Kim, T. W. and Choi, K.-S. *Science* 343, 990-994 (2014).
- [23] Chemelewski, W. D., Lee, H.-C. Lin, J.-F., Bard, A. J. and Mullins, C. B. *J. Am. Chem. Soc.* 136, 2843-2850 (2014).
- [24] Yu, Q., Meng, X., Wang, T., Li, P. and Ye, J. *Adv. Funct. Mater.* 25, 2686-2692 (2015).
- [25] Wang, T., Luo, W., Wen, X., Zou, Z. and Huang, W. *ChemNanoMat* 2, 652-655 (2016).
- [26] Kresse, G. & Furthmuller, J. *Comput. Mater. Sci.* 6, 15-50 (1996).
- [27] Blochl, P. E. *Phys. Rev. B* 50, 17953-17979 (1994).
- [28] Dudarev, S. L., Botton, G. A., Savrasov, S. Y., Humphreys, C. J. & Sutton, A. P. *Phys. Rev. B* 57, 1505-1509 (1998).
- [29] Faria, D. L. A., Silva S. V. and Oliveira, M. T. *J. Raman Spectrosc.* 28, 873-878 (1997).
- [30] Alexandrov, V. and Rosso, K. M. *J. Chem. Phys.* 140, 234701 (2014).
- [31] V. Balek and J. Subrt, *Pure Appl. Chem* 67, 1839-1842 (1995).
- [32] Lin, T.-C., Seshadri, G., Kelber, J. A. *Appl. Surf. Sci.* 119, 83-92 (1997).
- [33] Majzlan, J., Mazeina, L., Navrotsky, A. *Geochim. Cosmochim. Acta.* 71, 615-623 (2007).
- [34] Otte, K., Schmahl, W. W., Pentcheva, R. *Surf. Sci.* 606, 1623-1632 (2012).
- [35] Tang, C., Wang, H.-F., Wang, H.-S., Wei, F. and Zhang, Q. *J. Mater. Chem. A* 4, 3210-3216 (2016).